Heliyon 9 (2023) e23214

Contents lists available at ScienceDirect

Heliyon

journal homepage: www.cell.com/heliyon

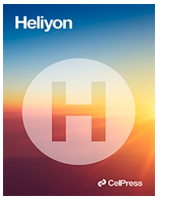

Multilayer amnion-PCL nanofibrous membrane loaded with celecoxib exerts a therapeutic effect against tendon adhesion by improving the inflammatory microenvironment

Chunjie Liu [a,b,c], Xiaochong Zhang [d], Lili Zhao [a,e], Limin Hui [f], Dengxiang Liu [g,h,*]

[a] Xingtai People's Hospital Postdoctoral Workstation, Xingtai People's Hospital, No.16, Hongxing Street, Xingtai 054031, China
[b] Postdoctoral Mobile Station, Hebei Medical University, No.361, Zhongshan Road, Shijiazhuang 050017, China
[c] Department of Orthopedics, Tangshan Workers Hospital, No.27, Wenhua Road, Tangshan 063000, China
[d] Department of Research and Education, Xingtai People's Hospital, No.16, Hongxing Street, Xingtai 054031, China
[e] Department of Orthopedics, Xingtai People's Hospital, No.16, Hongxing Street, Xingtai 054031, China
[f] Department of Gynecology, Xingtai People's Hospital, No.16, Hongxing Street, Xingtai 054001, China
[g] Institute of Cancer Control, Xingtai People's Hospital, No.16, Hongxing Street, Xingtai 054001, China
[h] Xingtai Key Laboratory of Precision Medicine for Liver Cirrhosis and Portal Hypertension, Xingtai People's Hospital, No.16, Hongxing Street, Xingtai 054001, China

ARTICLE INFO

Keywords:
Electrospun polyester membrane
Amniotic membrane
Anti-inflammation
Inflammatory microenvironment
Tendon adhesion

ABSTRACT

Tendon adhesion is a common complication after tendon surgery. The inflammatory phase of tendon healing is characterized by the release of a large number of inflammatory factors, whose mediated excessive inflammatory response is an important cause of tendon adhesion formation. Nonsteroidal anti-inflammatory drugs(NSAIDs) were used to prevent tendon adhesions by reducing the inflammatory response. However, recent studies have shown that the NSAIDs partially impairs tendon healing. Therefore, optimizing the anti-adhesive membrane loaded with NSAIDs to mitigate the effects on tendon healing requires further in-depth study. Amniotic membranes(AM) are natural polymeric semi-permeable membranes from living organisms that are rich in matrix, growth factors, and other active ingredients. In this study, we used electrostatic spinning technology to construct multifunctional nanofiber membranes of the PCL membrane loaded with celecoxib and AM. In vitro cellular assays revealed that celecoxib-loaded PCL membranes significantly inhibited the adhesion and proliferation of fibroblasts with increasing concentrations of celecoxib. In a rabbit tendon repair model, biomechanical tests further confirmed that the PCL membrane loaded with celecoxib had better anti-adhesion effects. Further experimental studies revealed that the PCL/AM membrane improved the inflammatory microenvironment by downregulating the expression of pro-inflammatory factors such as COX-2, IL-1β, and TNF-α proteins; and inhibiting the synthesis of COL I and COL III. The PCL/AM membrane can continuously release celecoxib to reduce the inflammatory response and deliver growth factors to the damaged area to build a suitable microenvironment for tendon repair, which provides a new direction to improve the repair efficiency of tendon.

* Corresponding author. Institute of Cancer Control, Xingtai People's Hospital, No.16, Hongxing Street, Xingtai 054001, China.
E-mail address: liudengxiang_1967@163.com (D. Liu).

https://doi.org/10.1016/j.heliyon.2023.e23214
Received 9 April 2023; Received in revised form 21 November 2023; Accepted 29 November 2023
Available online 3 December 2023

1. Introduction

With industrialization, the proportion of patients with hand injuries is 10%–30 % in emergency trauma cases [1,2]. The proportion of simple tendon injury or combined tendon injury is about 30 % [3]. Tendon adhesion of varying degrees can occur in approximately 10 % of patients with tendon injuries after surgical treatment. It seriously affects the functional rehabilitation of the affected finger, which has become an urgent problem to be solved in clinical practice [4–6].

Traditionally, tendon healing includes exogenous and endogenous healing. Endogenous healing is primarily achieved by self-proliferation of tendon cells and secretion of the extracellular matrix, whereas exogenous healing is achieved by the migration of fibroblasts from the tendon sheath and subcutaneous tissue around the injury to form granulation tissue at the damaged tendon [7]. Therefore, minimizing the factors of exogenous repair and allowing them to grow through endogenous healing are the key to avoiding adhesions.

Through in-depth research on tendon structure and adhesion mechanism, many methods and materials have been explored to prevent tendon adhesion, among which the placement of an anti-adhesive film to block exogenous healing remains the principal method to prevent tendon adhesions [8]. However, the anti-adhesion membrane can only play a limited physical barrier role, and cannot effectively prevent the adhesion of fibroblasts and inhibit the proliferation of adhesion tissue [9]. Moreover, trauma and surgery resulting in sterile or aseptic inflammation are risk factors for tendon adhesions.

The mechanism of adhesion formation is complex, and the inflammatory phase of tendon healing is characterized by the release of a large number of inflammatory factors, whose mediated excessive inflammatory response is an important cause of tendon adhesion formation [10]. Therefore, many scholars use nonsteroidal anti-inflammatory drugs to inhibit the inflammatory cells and factors associated with the development of adhesions to prevent tendon adhesions by reducing the inflammatory response. Recent studies have confirmed that ibuprofen effectively reduces the severity of tissue adhesions by blocking COX to inhibit macrophage infiltration, which in turn inhibits inflammatory factors such as TNF-α [11]. Celecoxib is not only a COX2 inhibitor but also an ERK2 phosphorylation inhibitor that inhibits TGF-β1-mediated ERK2 phosphorylation during joint adhesion formation, thereby inhibiting fibroblast proliferation [12]. Therefore, the controlled release of non-steroidal anti-inflammatory drugs in the nanofiber anti-adhesion membrane can be achieved using electrostatic spinning drug delivery technology, thereby promoting nutrient exchange while inhibiting cell adhesion and reducing the inflammatory response of tissues, laying the foundation for increasing the barrier capacity of the anti-adhesion membrane.

The researchers loaded celecoxib into an anti-adhesion membrane made of polyethylene glycol polylactide (PELA), and the slow release of the drug increased tendon adhesion inhibition, reduced neutrophil infiltration, and achieved good results in preventing adhesion formation. However, the tensile ultimate strength of the tendon at 3 weeks postoperatively by mechanical testing showed that the PELA fibrous membrane loaded with celecoxib group was obviously lower than the control group, suggesting that the released celecoxib incompletely damaged tendon healing [13,14]. Therefore, further research is needed to optimize the anti-adhesive membrane loaded with NSAIDs to mitigate the effects on tendon healing.

Amniotic membranes are natural polymeric semi-permeable membranes from living organisms that are smooth; free of blood vessels, nerves, and lymph; rich in the matrix, growth factors, enzymes, and other active components, making them ideal biomaterials [15–17]. Freeze drying can reserve the composition of the amniotic membrane and its richness in a variety of bioactive substance. Koob found by ELISA that a lyophilized amniotic membrane contains various growth factors such as bFGF, EGF, PDGF, TGF-βl and GCSF, which are important regulators in the healing of tendon injury [18]. Amniotic membranes, as natural biological alternatives, have specific advantages in many ways, including the construction of a tendon sheath, the inhibition of exogenous tendon healing, the promotion of endogenous healing, and the prevention of tendon adhesion, etc. The immunological, anti-inflammatory, antibacterial, and anti-adhesive properties of amniotic membranes will be further elucidated with the progress of biology and tissue engineering.

In this study, we proposed the construction of a multi-functional nanofiber composite membrane with polycaprolactone (PCL) nanofibers and amniotic membranes loaded with celecoxib by electrostatic spinning technology to investigate its inhibitory effect on tendon adhesion and explore its mechanism, thereby providing a new therapeutic method and theoretical basis for preventing tendon adhesion and promoting functional rehabilitation of the affected hand.

2. Materials and methods

2.1. Materials

2.1.1. Electrospinning of nanofibrous membranes

Approximately 0.5 g of gelatine from the porcine skinwere and 1 g of PCL dissolved in 10 mL of hexafluoroisopropanol with magnetic stirring. After complete dissolution, the mixture was left to stand overnight. The preparation method of celecoxib-PCL solution was to dissolve 0.05g, 0.08g and 0.10g celecoxib in PCL solution at concentrations of 5 %, 8 % and 10 %, respectively, as electrostatic spinning solutions.

The Department of Obstetrics and Gynecology, Third Hospital of Hebei Medical University, provided new amnions. Serological tests for HBV, HCV, HIV, syphilis, and gonorrhea in pregnant women were negative. The amnions were got after the pregnant woman and her family completed the consent form. The amnions were soaked in a balanced salt solution containing 50 μg/mL penicillin and 50 μg/mL streptomycin for 20 min. Put the fresh amnions in the freeze-drying chamber. Lyophilized amnions were sterilized using cobalt 60 irradiation.

At 25 °C ambient temperature and 60 % humidity, the electrostatic spinning device was assembled. The spinning solution was

poured into a syringe with a needle diameter of 0.7 mm, and the flow rate of the solution was set at 1.0 mL/h. The receiving distance was 15.0 cm, and the voltage was 13 kV. PCL nanofibers loaded with celecoxib (PCL/AM-5%, PCL/AM-8%, and PCL/AM-10 %) were received on the basolateral surface of lyophilized amniotic membranes, and PCL nanofibers without celecoxib were received on the epithelial cell surface, whereas PCL nanofiber membranes were prepared as experimental controls (Fig. 1A). The prepared different fiber membranes were placed in a vacuum vessel and dried overnight for use.

2.1.2. *Characterization of electrospun fibrous membranes*

The samples were gold-plated for 90 s, and then the morphology of PCL/AM, PCL/AM-5%, PCL/AM-8%, and PCL/AM-10 % membranes were observed using a scanning electron microscopy at an accelerated voltage of 10 kV. Image J software was used to analyze the SEM microscopy images. The diameters of 100 fibers were randomly calculated to evaluate the average diameter and diameter range of the fibers.

The porosity of PCL/AM nanofiber membrane was measured by ethanol permeation method. The initial volume of ethanol was marked as V1, and the volume was V2 after the nanofiber membrane was completely immersed in ethanol. After 15 min, the membrane was taken out of the ethanol, and the volume of residual ethanol was denoted as V3. The porosity of the tested membrane was contemplated using the following equation.

$$\text{Porosity}(\%) = \left(\frac{V_1 - V_3}{V_2 - V_3}\right) \times 100\%$$

Five samples with a size of 50.0 mm × 5.0 mm were collected and fixed on two mechanical clamps at both ends of the mechanical measuring instrument, reserving 3.0 mm as the testing area (MTS-Exceed-Model E42, MTS Systems Corporation, USA). The stretching rate was 0.5 mm/s. In addition, test results were averaged.

Water drops were placed on the surface of different samples. After 10 s, the hydrophilic angle tester was used to measure the hydrophilic angles of different fiber membranes at 25 °C, and the DSA 1.8 software was used to calculate.

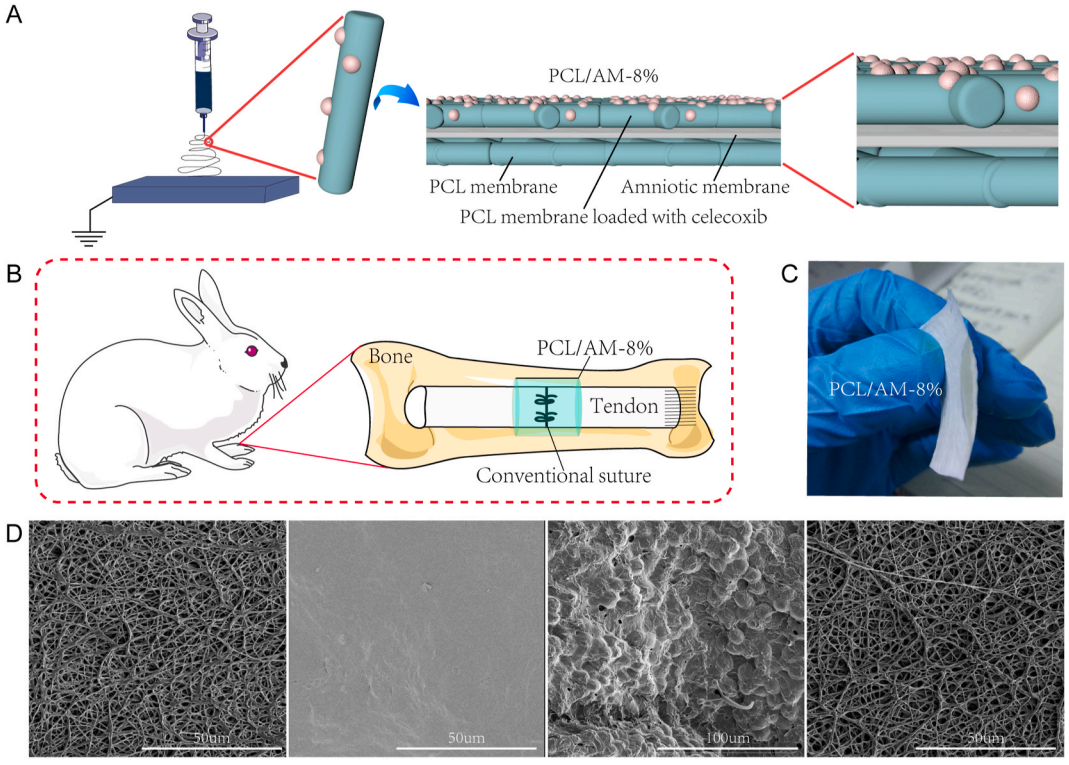

Fig. 1. (A) Schematic for the construction of a multilayer amnion-PCL nanofibrous membrane loaded with celecoxib by electrospinning. (B) Schematic diagram of amnion-PCL nanofibrous membranes loaded with celecoxib as the drug delivery systems and physical barriers for preventing tendon adhesion in rabbit models. (C) Appearance of the multilayer amnion-PCL nanofibrous membrane loaded with celecoxib. (D) The SEM micrographs of PCL nanofibrous membrane loaded with celecoxib, basement membrane surface, and epithelial cell surface of amniotic membrane, and PCL nanofibrous membrane. PCL membranes loaded with celecoxib and without celecoxib showed a nanofibrous morphology with an average thickness of around 0.15–0.2 mm. The thickness of amniotic membranes is about 0.04–0.06 mm.

2.2. Drug release study

Five pieces of the abovementioned four nanofiber membranes were collected and placed into 20 mL of phosphate-buffered saline (PBS). The suspension was placed in a 50 mL centrifuge tube and shaken at 100 rpm on a constant-temperature shaker. The drug-sustained release test was performed in an incubator at 37 °C. Five milliliters of supernatant was collected at different time intervals, and then 5 mL of fresh PBS was added. The drug concentration of celecoxib was measured by using a UV spectrophotometer at 249 nm wave peak, and the corresponding release curve was plotted. A linear correlation coefficient ($R^2 = 0.9917$) was obtained by comparing the absorbance of different concentrations of celecoxib standardized specimens (0, 2, 4, 6, 8, 10, and 14 μg/mL). According to the initial dose of celecoxib loaded into the membranes, the percentage of drug released from the membranes was measured.

2.3. 3. In vitro cell experiment

2.3.1. Isolation and culture of dermal fibroblasts

Six-month-old New Zealand white rabbits of either gender weighing 2.0–3.0 kg were provided by the Experimental Animal Center of the Hebei Medical University. Sodium pentobarbital (30 mg/kg) was injected into the ear vein and immobilised on the prone position. Under aseptic conditions, a palmar incision was made on the hind toe, and tissue surrounding the flexor tendon of the toe was excised. Specimens were rinsed three times with PBS containing double antibodies and put in DMEM containing 0.1 % type II catabolic enzyme overnight at 4 °C. The specimens were trimmed into 1 mm^3 pieces using ophthalmic scissors, put in DMEM containing 0.15 % collagenase NB4, and shaken for 2 h at 37 °C in a constant-temperature shaker. The mixture was filtered through a sterile filter to remove residual tissue and centrifuged at 200 g for 5 min. The supernatant was abandoned, and the cell precipitate was resuspended in DMEM culture medium containing 10 % FBS and 1 % double antibody. The cell suspension was put into the culture dish, and the dish was incubated at 37 °C with 5 % CO2 and 95 % air. The solution was replaced 2–3 times per week. Cells were observed daily for wall apposition, extension, and growth. When the cells proliferated and converged to 80 %, the cells were cultured in 1:2 equal fractions. Generations 3–5 were used for experimental studies.

2.3.2. Cell proliferation assessment

PCL, PCL/AM-5%, PCL/AM-8%, and PCL/AM-10 % membranes were put in 24-well plates, and another blank control group was set as well. Five groups were soaked in 75 % alcohol for 1 h, then alcohol was sucked and PBS was washed three times to clear residual alcohol. Fibroblasts were inoculated onto the materials at a density of $5*10^3$ cells/cm^2 and cultured in DMEM containing 10 % FBS and 1 % double antibodies. The cells incubated on different membranes were digested with 0.25 % trypsin on days 1 and 3, and the cell activity assay was performed using the CCK-8 method.

2.3.3. Cell fluorescence staining and adhesion test

On the first and third day of cell incubation, the fibroblasts were fixed with 4 % paraformaldehyde solution for 10 min, rinsed two times with PBS, and permeated using 200 pL of 0.1 % Triton X-100 solution for 10 min. The Triton X-100 solution was aspirated, and 20 μg/mL of phalloidin and 200 μL of 1 μg/mL DAPI were used sequentially for staining without light. The adhesion, cell growth, and cytoskeleton of cells on different membranes were observed and photographed by confocal laser microscopy.

2.4. Animal experiment

The protocols of the animal experiments were approved by the Ethics Board of the Third Hospital of Hebei Medical University, and all procedures were strictly followed the institutional guidelines for the care and treatment of experimental animals.

108 New Zealand rabbits (2–3 kg, male and female) in total, were randomly assigned into the control, AM, PCL, and PCL/AM-8% groups. There were 27 rabbits in each group. Rabbits were anesthetized with sodium pentobarbital (30 mg/kg). A short incision (1.5 cm) was performed between the metatarsophalangeal joint and the proximal interphalangeal joint of the third toe of the hindfoot under aseptic conditions. After the tendon sheath removal, the flexor digitorum profundus tendon was transected and sutured using the modified Kessler method. The tendons of the control group were sutured directly, and the other three groups were wrapped around the suture with a freeze-dried amniotic membrane, PCL membrane, and PCL/AM-8% membrane (Fig. 1B). After surgery, the lower limbs were immobilised, stayed warm and put in separate cages to ensure enough diet. Intramuscularly injected penicillin (400000U) once a day for 3 days.

2.4.1. Gross observation

The animals were executed by an intravenous overdose of sodium pentobarbital 3 weeks after the surgery. A total of nine animals were included in each group at each time point. The third toes were obtained from nine rabbits at each time point in each group. Tendon healing and adhesion to the surrounding tissue were evaluated. Tendon adhesion and healing were evaluated in accordance with standards made by Yang and Tang et al. [4,19].

2.4.2. Biomechanical evaluation

Skin and fur were removed, and the metacarpophalangeal joint was mechanically dissociated 3 weeks after surgery. Mechanical properties, including the tendon's total flexion angle and maximum tensile strength, was calculated using a biomechanical testing machine. The third toe's proximal phalanx was attached to the testing machine. The remaining flexor digitorum profundus tendon was

tractioned with 1 N force, and the traction force was increased at a constant rate until 10 N. A protractor was used to measure the total flexion angle. The proliferative tissues surrounding the deep flexor tendon were removed. On a biomechanical testing machine, both ends of the deep flexor tendon were immobilised. The tendon was moved at 20 mm/N until it ruptured, and the maximum tensile rupture strength of the tendon was recorded concurrently.

2.4.3. Western blot analysis

The adherent tissue was collected and placed into a 1.5 mL centrifuge tube. After adding 200 UL of Ripa lysate, 1 UL of PMSF, 2 UL of phosphatase inhibitor, and 2 UL of protease inhibitor, they were placed in a tissue homogenizer. The tissue was homogenized for 2 min until it was fully broken and then placed on ice for 30 min. After centrifugation at 12,000 rpm for 10 min at 4 °C, the supernatant was put in a new 1.5 mL centrifuge tube and kept on ice. BCA protein concentration determination kit was used to determine the total protein concentration of different samples. The samples were electrophoresed through a 10 % SDS-PAGE gel and then transferred onto a PVDF membrane. After being blocked with 5 % skim milk powder, the membranes were incubated with antibodies against COX2, COL-I, COL-III (Bioss, China), TNF-α (Novus,USA), α-SMA (Abcam, USA), IL-1β (Proteintech,USA), and GAPDH (Bioss, China) at 4 °C overnight. After cleaning with Tris-buffered saline (TBS) 3 times, the secondary antibody was added and incubated for 2 h at room temperature. The membrane was washed three times with TBST (50 mL of Tris-HCl, 100 mL of NaCl, and 0.1 % Tween-20, pH 7.4) and scanned using the Odyssey Fc System (LICOR, USA). The densitometry of bands was measured by Image-Pro Plus 6.0 software (Media Cybernetics, USA).

2.4.4. Immunohistochemistry

Adherent tissues were formalin-fixed, paraffin-embedded, sectioned, dewaxed, hydrated, and closed using goat serum after antigen repair. CD68, TNF-α (Novus,USA), IL-1β, α-SMA (Proteintech,USA), COX2 and COL-III (Bioss, China) antibodies were added dropwise overnight at 4 °C. After incubation with secondary antibody, color development was performed by DAB staining and Harris hematoxylin counterstaining. Images were acquired using an Olympus optical camera system, and five randomly captured images were collected at each section. A brownish-yellow color was considered positive. The mean optical density values (IOD/area) of each group were measured and calculated using Image-Pro Plus 6.0 software.

2.5. Statistical analysis

The mean ± standard deviation was used to calculate the results. Differences among the experimental groups were evaluated using one-way analysis of variance with SPSS 24.0 software (SPSS, Chicago, USA). Differences were considered significant at $P < 0.05$. Comparisons with no statistically significant differences are not marked in the figures.

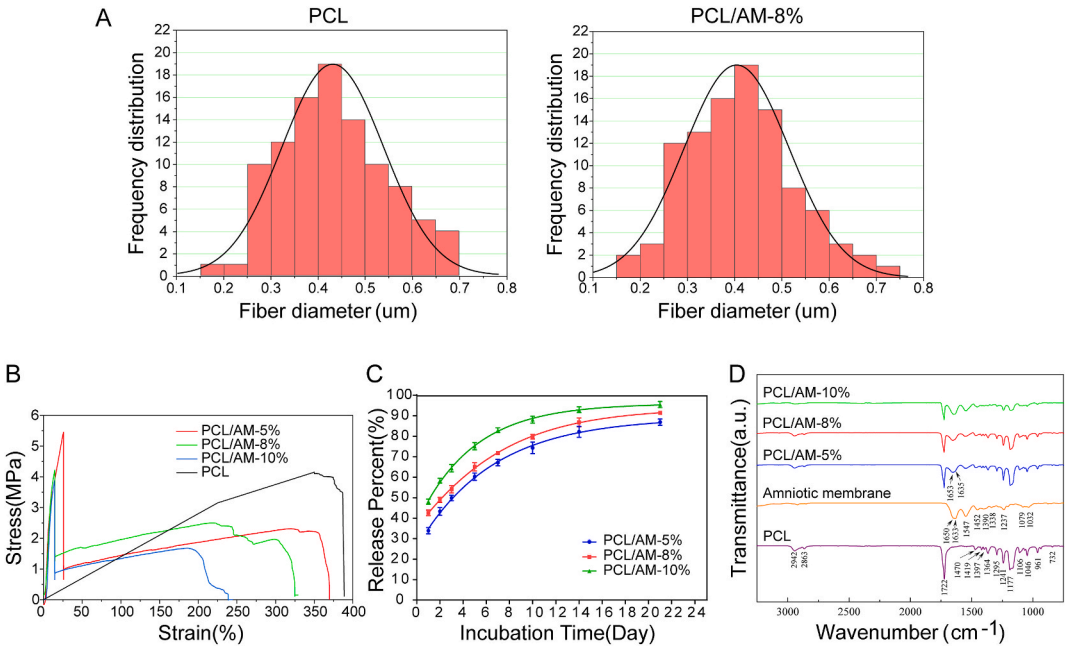

Fig. 2. (A) Histograms showing the diameter distributions of the PCL nanofibrous and celecoxib-loaded PCL nanofibrous membranes based on SEM observations. (B) Mechanical estimation of stress–strain curved lines for PCL nanofibrous membranes. (C) The accumulative release percentage of loaded celecoxib from PCL/AM-5%, PCL/AM-8%, and PCL/AM-10 % membranes. (D) The FTIR spectra of the PCL/AM-8%, amniotic, and PCL nanofibrous membranes.

3. Results

All the uncropped original blot images are presented as Supplemental Figures.

3.1. Characterization of electrospun nanofiber membranes

Appearance of the multilayer amnion-PCL nanofibrous membrane loaded with celecoxib (Fig. 1C). SEM was used to characterize the morphology of PCL/AM, PCL/AM-5%, PCL/AM-8%, and PCL/AM-10 % electrospun nanofibers. The structure of lyophilized amniotic epithelial cells was intact, the cell space was enlarged, the surface was flat, the drying shrinkage was slight, and the intercellular connection structure was clear. The basement membrane surface was smooth, and the structure of collagen fibers in the matrix was clear (Fig. 1D).

The nanofibers of all samples were uniform in diameter, continuous, smooth, and free of beads. The average diameter of different PCL nanofibers decreases with the increase of celecoxib content. The average diameters of PCL, PCL-5%, PCL-8%, and PCL-10 % nanofibers were 0.43 ± 0.11 μm, 0.41 ± 0.09 μm, 0.40 ± 0.11 μm, and 0.39 ± 0.12 μm (Fig. 2A). The porosity of PCL, PCL/AM-5%, PCL/AM-8%, and PCL/AM-10 % nanofiber membranes gradually increased, which were 68.32 % ± 2.95 %, 74.54 % ± 3.60 %, 78.44 % ± 1.29 %, and 80.68 % ± 3.52 %. Moreover, the hydrophilic angles were 112.70° ± 4.76°, 63.64° ± 2.55°, 71.12° ± 3.33°, and 73.32° ± 2.49°, respectively.

PCL, PCL/AM-5%, PCL/AM-8%, and PCL/AM-10 % nanofiber membranes were all elastic. During the mechanical property test, the membranes were gradually elongated, and the middle part was gradually narrowed. The PCL/AM-5%, PCL/AM-8%, and PCL/AM-10 % membranes initially underwent fracture of the internal amniotic membrane and eventually broke down. The deformation rate of the PCL membrane loaded with celecoxib decreased compared with that of the PCL membrane. The maximum tensile strength and deformation rate decreased gradually with the increase of celecoxib content. The maximum tensile strengths of PCL, PCL/AM-5%,

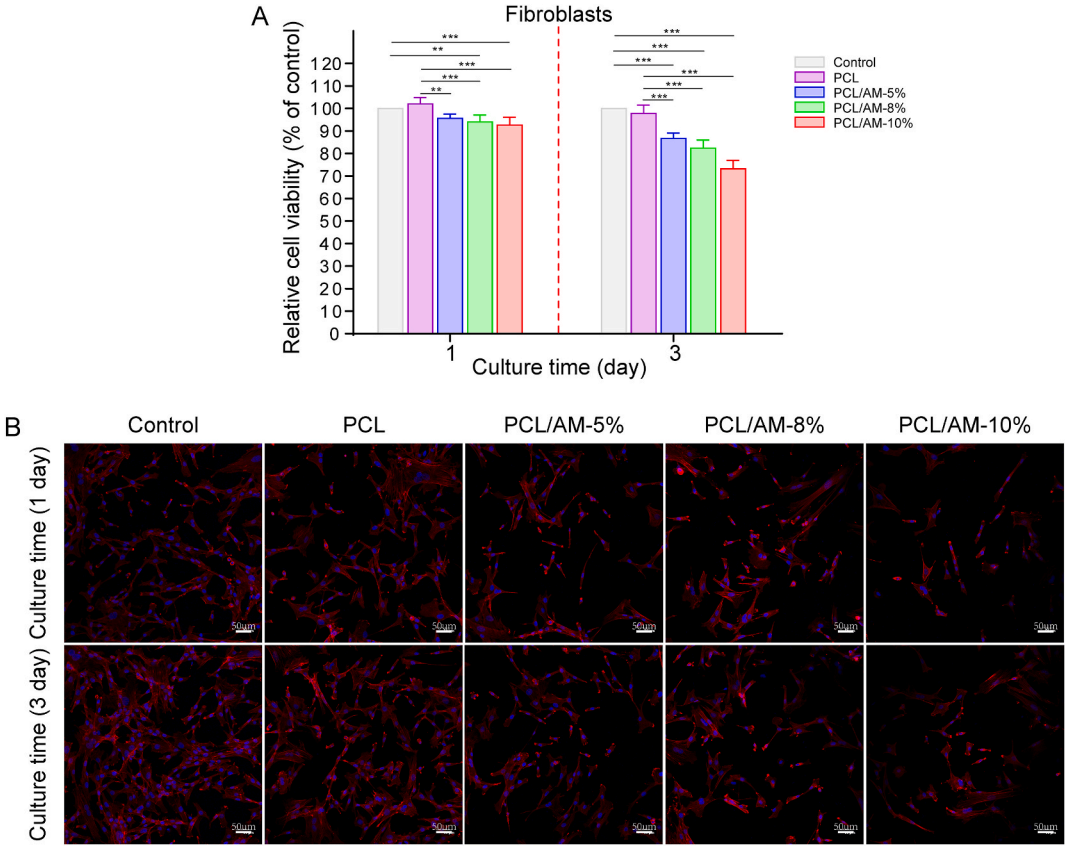

Fig. 3. Cytotoxicity of membranes loaded with different contents of celecoxib by culture fibroblasts on PCL, PCL/AM-5%, PCL/AM-8%, and PCL/AM-10 % membranes for 1 and 3 days. (A) The relative cell viability was standardized with cells incubated in fresh cell culture medium (control), which was considered to be 100 %.(B) Attachment and proliferation of fibroblasts on the surface of various membranes. Fluorescent photographs of fibroblasts of culture on PCL, PCL/AM-5%, PCL/AM-8%, and PCL/AM-10 % membranes at days 1 and 3. The nucleuses were stained blue with DAPI, and the actin cytoskeleton were stained red with phalloidin.Bar = 50 μm. Data are expressed as mean ± SD. $p < 0.05$ considered significant. *: $p < 0.05$; **: $p < 0.01$; ***: $p < 0.001$. (For interpretation of the references to color in this figure legend, the reader is referred to the Web version of this article.)

PCL/AM-8%, and PCL/AM-10 % membranes were 4.12 ± 0.15 MPa, 5.14 ± 0.52 MPa, 4.08 ± 0.18 MPa, and 4.09 ± 0.25 Mpa, respectively, and the deformation rates were 394.60 ± 20.26, 354.20 ± 20.24, 307.10 ± 22.42, and 253.70 ± 12.61, respectively (Fig. 2B).

Membranes loaded with different levels of celecoxib could achieve sustained release of the drug. At the beginning of the drug release experiment, PCL/AM-5%, PCL/AM-8%, and PCL/AM-10 % membranes showed a sudden release with 35.1 %, 41.1 %, and 46.9 % of celecoxib released, respectively. In the following 2 weeks, the release of celecoxib tended to be slow and stable. With the increase of celecoxib concentration, the drug release rate gradually accelerated. After 3 weeks, celecoxib was almost completely released from the membranes (Fig. 2C).

The infrared spectrum of the PCL membrane was dominated by typical ester and hydrocarbon bonds, including two peaks at 2942 and 2863 cm^{-1}, corresponding to the stretching vibration of CH_2. The absorption peak at 1722 cm^{-1} was due to carbonyl stretching vibration. The antisymmetric bending vibration peak of CH_2 was at 1470 cm^{-1}, and the two absorption peaks of 1397 and 1364 cm^{-1} belonged to the symmetrical bending vibration of CH_2. In addition, the bending vibration of O–CH_2 was 1419 cm^{-1}. The absorption peaks at 1295, 1241, 1177, and 1106 cm^{-1} were due to C–O–C stretching vibration. The vibration of the O[CH_2]$_5$ isomer was 1046 cm^{-1}. Moreover, the *trans*-C-O symmetric telescopic vibration was 961 cm^{-1}, and the CH_2 in-plane rocking vibration was 732 cm^{-1}.

The proteins contained in the freeze-dried amniotic membrane had many characteristic absorption peaks in the infrared spectrum. The characteristic absorption peaks of the amide I and II bands were 1650–1630 and 1547 cm^{-1}, respectively. After fitting and splitting the absorption peaks in this range, the secondary structures corresponding to 1650 and 1633 cm^{-1} were α-helical and β-folded structures, which were due to the vibrations of two C═O groups that had joined hydrogen bonds. The absorption peak at 1452 cm^{-1}

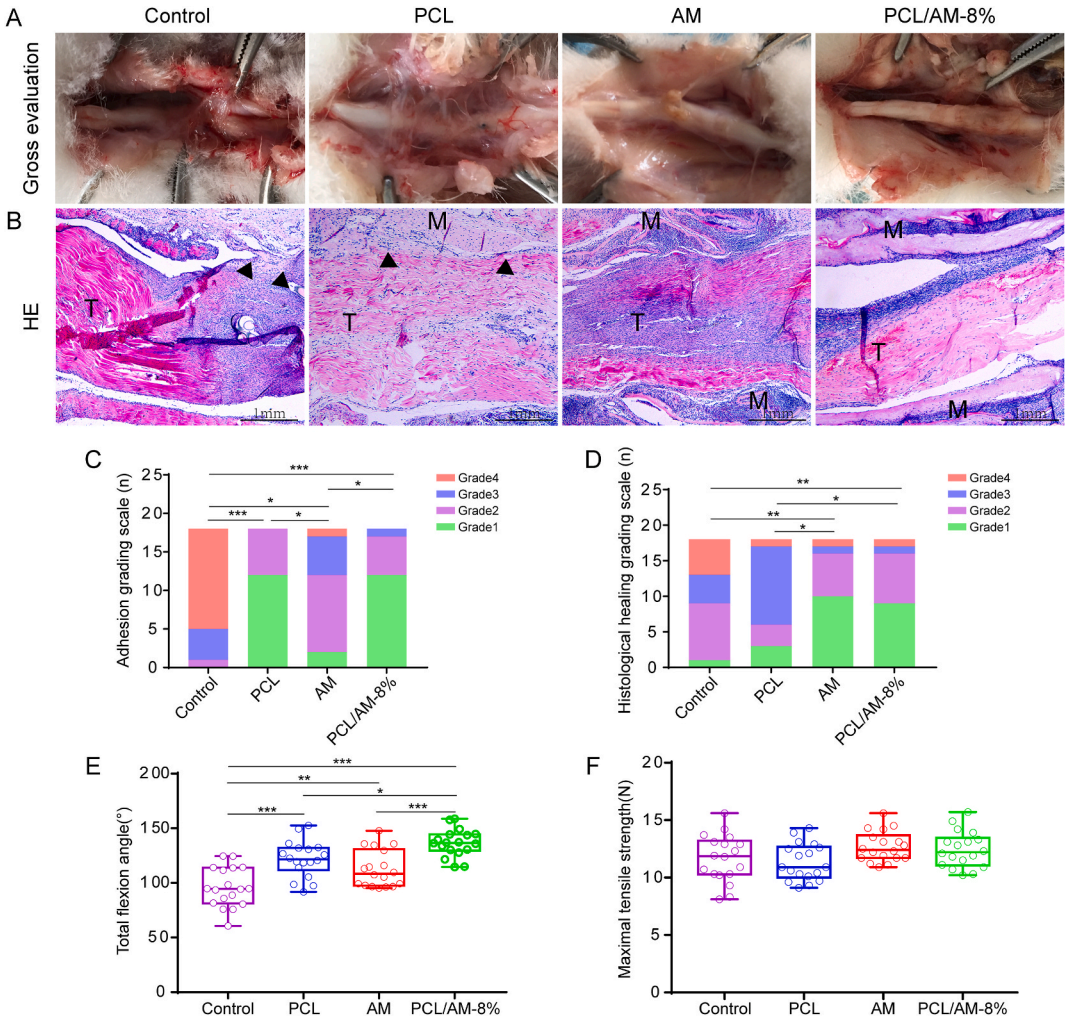

Fig. 4. (A) Gross views of the rabbit tendons with different levels of adhesion in the untreated control, PCL, AM, and PCL/AM-8% groups 3 weeks after surgery. (B) Histological analysis by hematoxylin-eosin staining was performed to evaluate adhesion formation. T: tendon; M: membrane. The black triangle indicates the adhesive tissue. The peritendinous adhesions and healing quality were analysed on the basis of gross observation (C), histological analysis (D), flexion angle of interphalangeal joint (E), and maximum tensile fracture strength (F) 3 weeks after surgery. *: $p < 0.008$; **: $p < 0.0016$; ***: $p < 0.0001$.

corresponded to the stretching vibration of the C–N bond. Bending vibration corresponding to CH_3 was 1390 cm^{-1}. The bending vibration of CH_2 was 1338 cm^{-1}. In addition, the absorption peak of amide III band was 1237 cm^{-1}, and the corresponding protein secondary structure was a β-folding structure. The characteristic peak of C═O bending vibration was 1079 cm^{-1}. Moreover, the characteristic peak at 1032 cm^{-1} was produced by the stretching vibration of C–O on the serine side chain.

The infrared spectrum of the composite PCL/AM membrane showed that both characteristic peaks belonged to the outer PCL membrane and inner amnion. No other new characteristic peaks were observed. Notably, the absorption peak of the amide I band of the composite membrane was blue-shifted compared with that of the freeze-dried amniotic membrane (Fig. 2D).

3.2. In vitro cell study

Fibroblasts could adhere and proliferate on PCL, PCL/AM-5%, PCL/AM-8%, and PCL/AM-10 % membranes, and the number of cells increases gradually with the extension of time. Cells grew poorly on PCL/AM membranes loaded with celecoxib, and the activity gradually reduced with growing celecoxib concentration. On the 1st day of culture, the activity of fibroblasts on PCL/AM-8% and PCL/AM-10 % membranes was lower than that on control and PCL membranes. On the 3rd day of culture, the activity of fibroblasts on PCL/AM-5%, PCL/AM-8%, and PCL/AM-10 % membranes was obviously lower than that of fibroblasts on control and PCL membranes. Thus, PCL membranes loaded with celecoxib significantly inhibited the activity of fibroblasts (Fig. 3A).

Cell fluorescence staining and adhesion test showed that the area of fibroblasts on the culture plate of the control group was the largest. Compared with the control and PCL groups, the area of fibroblasts on the PCL membrane loaded with celecoxib decreased, and the spreading area of fibroblasts on the PCL/AM-10 % membrane was the smallest. Thus, the PCL membrane loaded with celecoxib inhibited the adhesion of fibroblasts (Fig. 3B).

3.3. In vivo studies

Three weeks after operation, the wound healed well in all groups, and no infection or ulcer appeared. The tendon was exposed after separation of the skin and surrounding soft tissues. Tendon adhesions were assessed by gross observation. Dense adhesive tissue

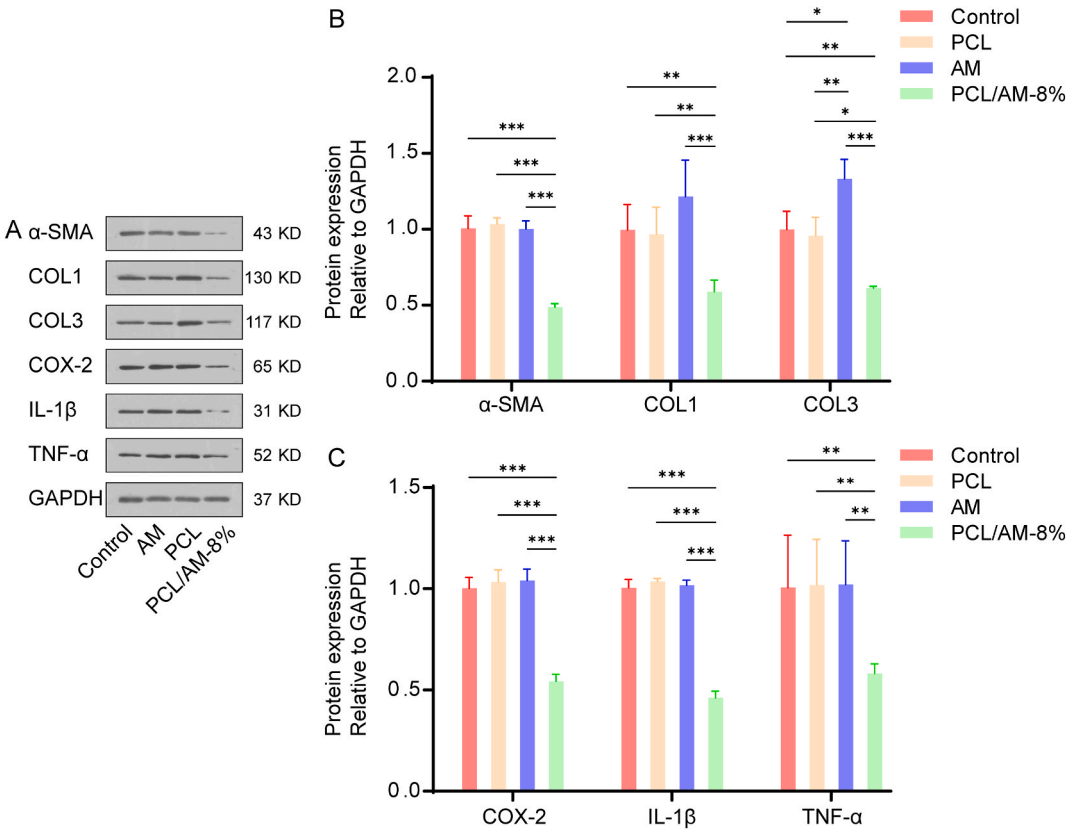

Fig. 5. Western blotting assay for α-SMA, COL-I, COL-III, COX-2, TNF-α, and IL-1β expression in repair sites with the control, PCL, AM, and PCL/AM-8% groups 3 weeks after operation (A). Densitometry of α-SMA, COL-I, COL-III (B), COX-2, TNF-α, and IL-1β (C) from Western blot experiment. GAPDH expression was included as a loading control. Data are expressed as mean ± SD. $p < 0.05$ considered significant. *: $p < 0.05$; **: $p < 0.01$; ***: $p < 0.001$.

appeared around the repaired tendon in the control and AM groups. The surgical suture had been wrapped by adherent tissue in the control group, which could not be observed, requiring a sharp instrument to separate it. In the AM group, the amniotic membrane was not completely tiled, and it locally bulged into a mass, which was difficult to identify. By contrast, in the PCL group, the surgical suture was clearly visible. Between the tendon and the surrounding tissue, a small amount of fibrous tissue adhered. Almost no adhesive tissue formation was observed in the PCL/AM-8% group (Fig. 4A). A statistically significant difference in the degree of tendon adhesion was observed between the PCL/AM-8% and PCL groups compared with the control and AM groups, whereas no statistical differences were observed between the PCL/AM-8% and PCL groups (Fig. 4C).

HE staining of tissue sections of the repaired tendon showed that the tendon in the control group was tightly adherent to the surrounding granulation tissue, which severely affected tendon healing. The PCL group showed peritendinous fibrotic tissue between tendon and surrounding soft tissue. The collagen fibers within the tendon showed good repair in the AM group, but loose bundles of fibrous tissue adhered to the flexor tendon sheath. By contrast, the collagen fibers were successive at the tendon repair in the PCL/AM-8% groups, with little adhesion and a obvious gap between the tendon and surrounding tissue (Fig. 4B). The quality of tendon healing was significantly better in the PCL/AM-8% and AM groups than in the control and PCL groups, with statistically significant differences (Fig. 4D).

In this study, the range of motion (ROM) was measured to reflect the degree of tendon adhesions. The larger the ROM, the lesser the adhesion. The total flexion angles in the PCL/AM-8% groups, AM groups, and PCL groups were increased compared with the control group, particularly the PCL/AM-8% group, which was the most significantly improved, with statistically significant differences

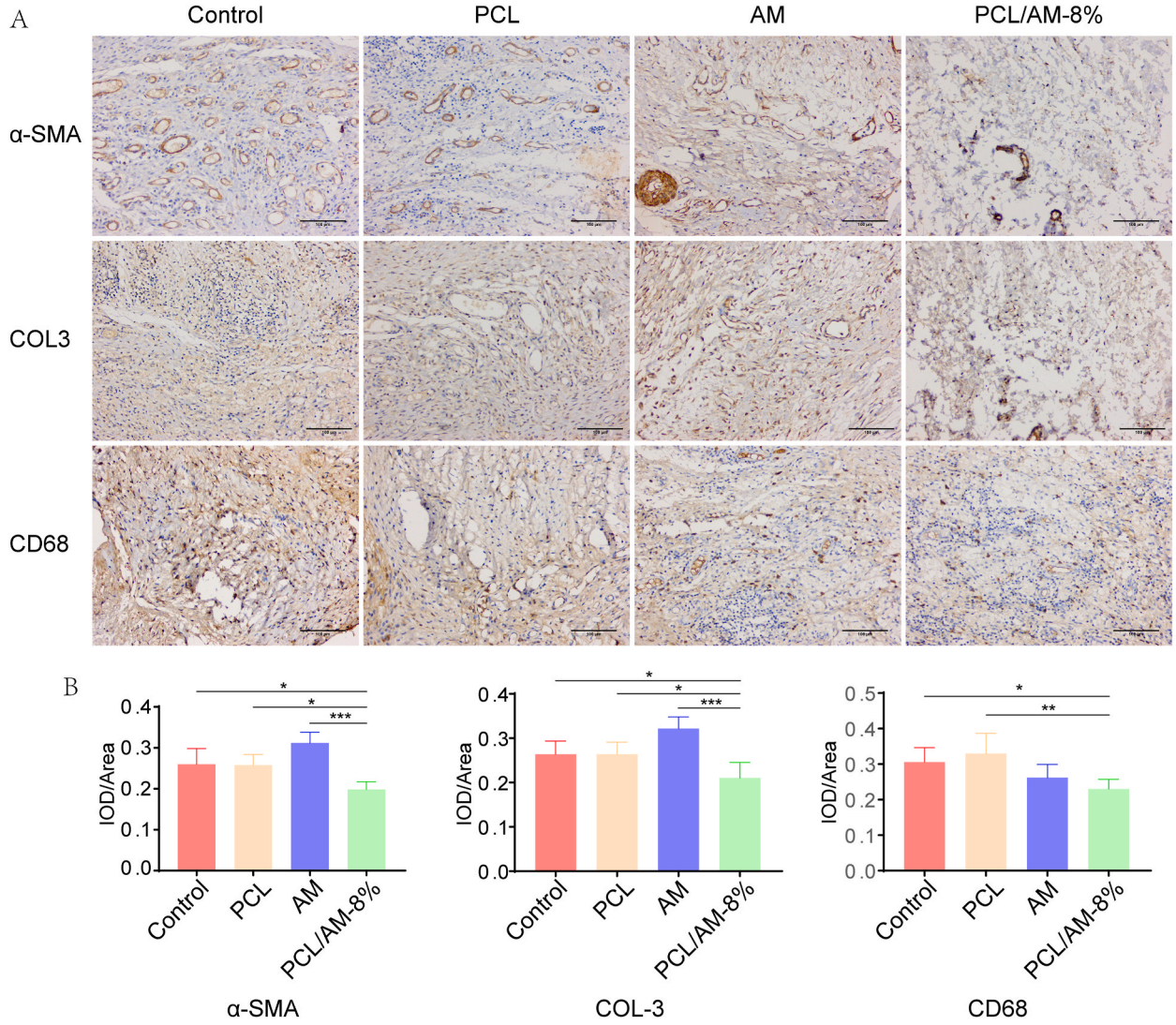

Fig. 6. (A) Immunohistochemical staining photos for α-SMA, COL-III, and CD68 expression in the repaired sites of tendons with the control, PCL, AM, and PCL/AM-8% groups 3 weeks after surgery. (B) The average optical density of α-SMA, COL-III, and CD68. IOD, integrated optical density. *: $p < 0.05$; **: $p < 0.01$; ***: $p < 0.001$.

(Fig. 4E). The maximum tensile rupture strength of the tendon can reflect the healing of the tendon to a certain extent. The maximum tensile rupture strength of the tendon in the PCL/AM-8%, AM, PCL, and control groups was close and not statistically different (Fig. 4F).

In exploring the mechanism of the multilayer PCL/AM membrane loaded with celecoxib to prevent tendon adhesions and promote endogenous tendon healing, the expression of α-SMA, COL I, COL III, COX-2, IL-1β, and TNF-α proteins in tendon repair tissues was detected by immunoblotting 3 weeks after operation, and GAPDH was used as an internal reference (Fig. 5A & Supplemental Figures). The PCL/AM-8% group loaded with celecoxib had significantly lower expression of α-SMA and COL I than the other three groups and lower COL III expression than the AM group. By contrast, the AM group showed significantly higher expression of α-SMA, COL I, and COL III than the other three groups (Fig. 5B). These results indicate that celecoxib blocks the expression of α-SMA, COL I, and COL III; however, the amniotic membrane can attenuate this tendency and improve the quality of tendon healing.

Tendon repair after injury cannot be achieved without its specific immune microenvironment. The PCL/AM-8% group loaded with celecoxib had significantly lower expression of COX-2, IL-1β, and TNF-α proteins than the other three groups ($p < 0.05$), and these inflammatory mediators were important factors in the immune microenvironment to improve tendon healing quality and reduce adhesions (Fig. 5C).

Celecoxib may reduce tendon adhesions by improving the immune and inflammatory microenvironment. In this study, an immunohistochemical method was used to detect COL III and neovascular markers related to inflammation in tendon repair area α-SMA, macrophage marker CD68, and pro-inflammatory factors such as COX-2, IL-1β, and TNF-α. Compared with the control, PCL,

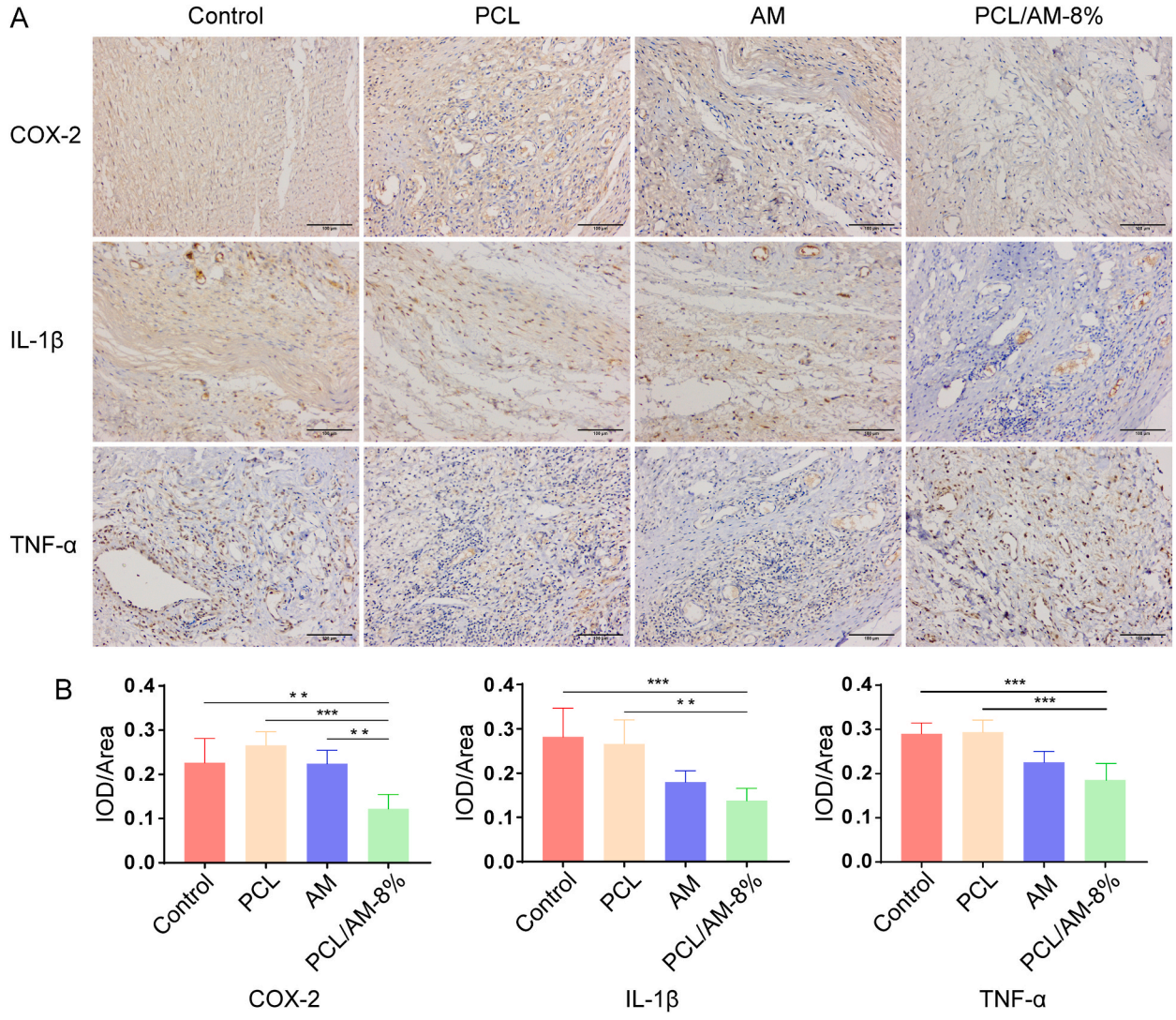

Fig. 7. (A) Immunohistochemical staining photos for COX-2, TNF-α, and IL-1β expression in the repaired sites of tendons with the control, PCL, AM, and PCL/AM-8% groups 3 weeks after operation. (B) The average optical density of COX-2, TNF-α, and IL-1β. IOD, integrated optical density. *: $p < 0.05$; **: $p < 0.01$; ***: $p < 0.001$.

and AM groups, α-SMA and COL III were less distributed in the PCL/AM-8% group with significant differences. Macrophage aggregates were observed in the tissues of specimens from all groups receiving different treatments, which were less in the PCL/AM-8% and AM groups than in the control and PCL groups (Fig. 6A). α-SMA, COL III, and CD68 per unit area were measured for semi-quantitative analysis (Fig. 6B). Celecoxib, as a selective COX-2 inhibitor, significantly reduced COX-2 expression in the PCL/AM-8% group compared with the other three groups, whereas IL-1β and TNF-α expression in the PCL/AM-8% and AM groups was lower than that in the control and PCL groups (Fig. 7A and B).

4. Discussion

Tendon injuries are common in sports. Given the low content of cells, blood vessels, and nerves in tendon tissue and poor self-repair ability, complications such as tendon adhesions can easily occur. Unlike other COX inhibitors, celecoxib not only selectively inhibits

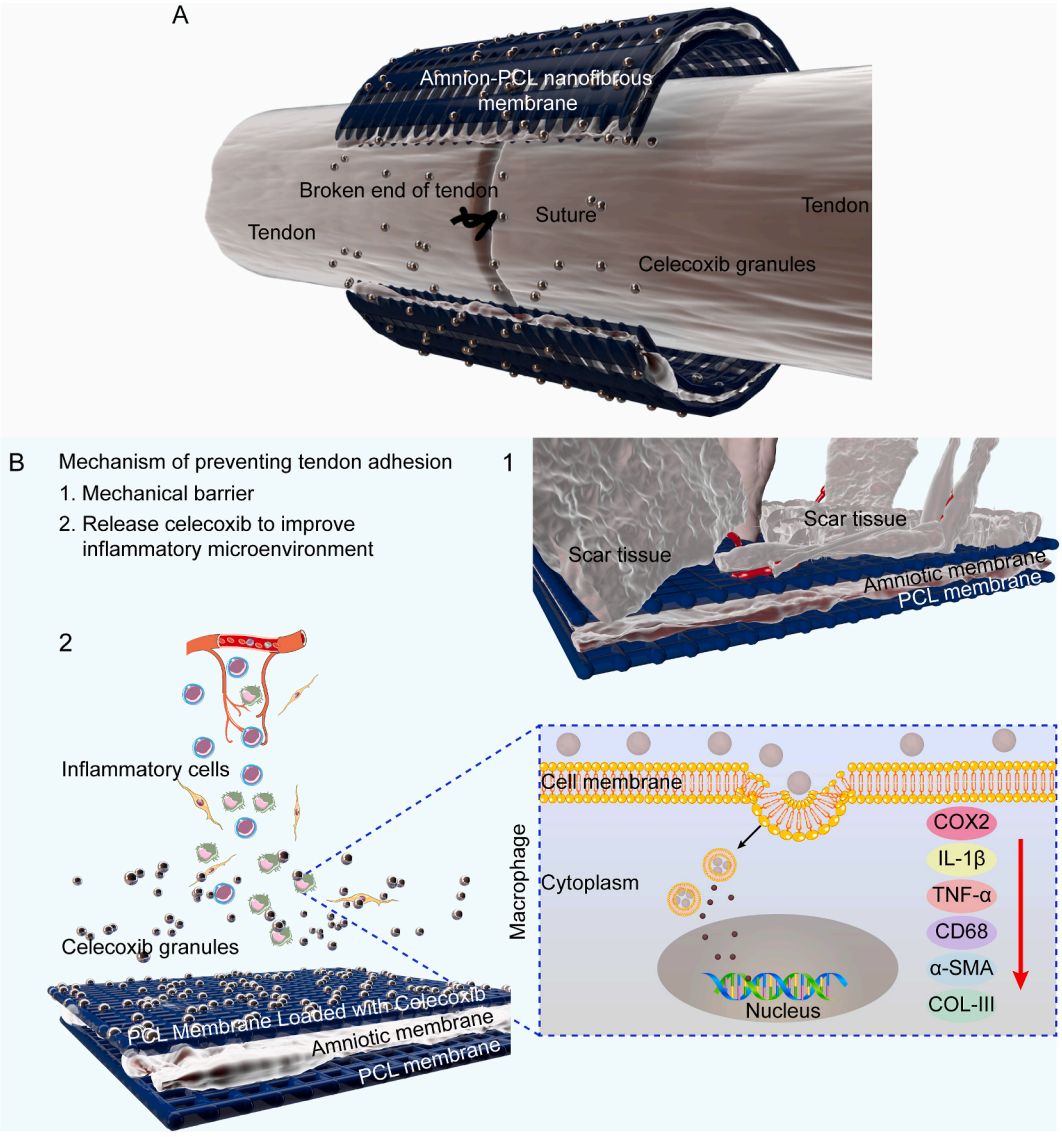

Fig. 8. Schematic drawing of the mechanism of the multilayer amnion-PCL nanofibrous membrane loaded with celecoxib as the drug delivery systems and physical barriers for preventing tendon adhesion. (A). The healing process of tendons after surgery involves very complex interactions between the tendon proper and inflammatory microenvironment. In general, excessive inflammatory response leads to scar tissue proliferation that fails to rebuild tissue boundaries. The absence of compartmentalization may adversely result in tendon adhesion. A PCL/AM-8% physical barrier can prevent peritendinous adhesion. After tendon injury, the extrinsic healing mechanism (vasculature, nerve, and immune cells) is activated in early stages of healing. After implantation of PCL/AM-8% membranes in the rabbit model, celecoxib was released continuously. A decrease in macrophage infiltration, α-SMA positive vessels, COX-2, TNF-α, IL-1β expression, and COL III deposition was detected (B).

COX-2, but also plays a role in anti-angiogenesis and anti-fibrosis [20,21]. Given its advantages, the PCL membrane loaded with celecoxib can not only prevent or reduce adhesions through the barrier effect of the membrane, but also achieve a better anti-adhesion effect by affecting the exogenous healing mechanism of the tendon through the pharmacological effect of celecoxib. However, recent studies have shown that the released celecoxib partially impairs tendon healing [14]. Therefore, how to optimize the anti-adhesive membrane loaded with NSAIDs to mitigate the effects on tendon healing requires further in-depth study.

In this study, we used electrostatic spinning technology to compose multi-layered nanofiber membranes of the PCL membrane loaded with celecoxib and amniotic membrane, which had good drug-sustained release ability, and it can weaken the sudden release phenomenon of drugs. The experiment showed that celecoxib was almost completely released from the composite membrane after 3 weeks, which was consistent with the time of exogenous healing after tendon injury. In vitro cellular assays revealed that celecoxib-loaded PCL membranes significantly inhibited the adhesion and proliferation of fibroblasts with increasing concentrations of celecoxib. In a rabbit tendon repair model, biomechanical tests further confirmed that the PCL membrane loaded with celecoxib had better anti-adhesion effects. Moreover, the maximum tensile rupture strength of the tendon did not show a significant decrease. In exploring the possible pathological mechanisms by which the celecoxib-loaded PCL/AM-8% composite membrane inhibits exogenous healing and promotes endogenous healing, further experimental studies revealed that the composite material reduced peritendinous inflammation and improved the inflammatory microenvironment by reducing macrophage aggregation; downregulating the expression of pro-inflammatory factors such as COX-2, IL-1β, and TNF-α proteins; and inhibiting the synthesis of COL I and COL III (Fig. 8A and B).

Electrostatically spun fibers have a high surface-to-volume ratio, adjustable porosity, and ductility, and the diameter of electrostatically spun fibers is similar to that of extracellular matrix fibers. Therefore, electrostatically spun tissue engineering scaffolds can mimic the extracellular matrix microenvironment [22,23]. In this study, a new amniotic membrane/PCL nanofiber scaffold loaded with celecoxib was constructed by electrostatic spinning, which is hoped to be a breakthrough in solving tendon adhesion. The results showed that the PCL membrane had good mechanical properties, which were consistent with the high tensile strength of tendon tissue; the slow and sustained release of celecoxib inhibited the adhesion of fibroblasts, and the release of various bioactive factors from the amniotic membrane promoted endogenous tendon healing. These data indicate that the PCL/AM-8% composite material has the essential function and structure of the material that is required for this subject. Compared with other PCL membranes loaded with celecoxib, the PCL/AM-8% composite membrane has a moderate drug content, slow drug release, and inhibition of fibroblast proliferation, which is suitable for preventing tendon adhesions and avoiding excessive damage to tendon healing. Therefore, we applied it to animals in vivo.

Effective tissue repair is essential for the functional rehabilitation of the limb. Tendon injury activates a local inflammatory response, which can lead to the release of chemokines [24]. Neutrophils, macrophages, and other intrinsic immune cells are recruited to the site of injury to remove necrotic cells and tissue and subsequently participate in tissue repair. Differences in the degree and duration of the inflammatory response can lead to different repair outcomes. The inflammatory response is like a double-edged sword. On the one hand, it promotes wound closure and tissue healing through fibrous proliferation; on the other hand, inflammation induces scar tissue proliferation triggering complications such as tendon adhesions [25,26].

Macrophages are a major source of pro-inflammatory factors in the early stages of tendon repair [27]. Cytokines secreted by macrophages are closely associated with inflammatory responses and adhesive tissue proliferation, but the exact mechanism of macrophage action in adhesions is unknown. Macrophages promote inflammatory responses by expressing COX genes to produce prostaglandins and by secreting different cytokines such as IL-1β and TNF-α [28]. As a selective COX-2 inhibitor, celecoxib has shown better inhibition of intra-abdominal adhesions and joint adhesions than ibuprofen or other nonsteroidal anti-inflammatory analgesics in previous studies [29,30]. In addition, the non-selective COX-2 inhibitor (ibuprofen) has side effects caused by COX-1 inhibition, including gastrointestinal and renal damage and bleeding caused by inhibition of platelet aggregation [31]. Unlike other COX inhibitors, celecoxib has anti-angiogenic and anti-fibrotic properties in addition to its COX-2 inhibitory effects, and these pharmacological activities may enhance the inhibitory effect of celecoxib on tendon adhesion formation.

At different stages of tendon healing, macrophages exhibit two completely different cell phenotypes, namely, M1 and M2, both of which play completely different roles [32]. The early stage of tissue healing is dominated by M1-type macrophages, which secrete pro-inflammatory factors such as IL-1β and TNF-α to clear pathogens and provide a suitable microenvironment for the infiltration of inflammatory cells. An acute inflammatory response occurs in the repaired area after tendon injury. A large number of macrophages infiltrate and highly express pro-inflammatory factors such as IL-1β and TNF-α to enhance the local inflammatory response, stimulate cell division, chemotaxis a large number of fibroblasts gathered to the damaged area, over-secrete COL I and COL III, and deposit them in large quantities, leading to the formation of adhesions [33,34]. However, excessive adherent tissue can impede endogenous tendon healing and tissue remodeling. Therefore, proper reduction of the inflammatory response and improvement of the microenvironment for tendon repair can improve endogenous tendon healing and reduce complications such as tendon adhesions. In this research, the PCL/AM-8% nanofiber composite membrane reduced macrophage infiltration, downregulated the expression of pro-inflammatory factors such as IL-1β and TNF-α, and reduced collagen synthesis through the sustained release of celecoxib, thereby obtaining good results in limb function recovery.

The PCL membrane loaded with celecoxib has an inhibitory effect on fibroblasts and tenocytes; thus, the inhibition of tendon adhesions may occur along with a reduction in the quality of tendon repair. Therefore, we incorporated the amniotic membrane into the middle layer of the composite membrane to release multiple growth factors and promote endogenous tendon healing. Human amniotic membrane is derived from discarded placental tissue, and it is the innermost of the placenta, which is approximately 0.02–0.5 mm thick. Its wide source, inexpensive, very low immunogenicity, lack of tumorigenicity, and ethical controversy make it an optimal biomaterial for trauma repair [35,36]. Researchers have applied connective tissue growth factor(CTGF), growth

differentiation factor(GDF), and transforming growth factor (TGF-β) to tendon repair experiments [37–39]. Although some results have been achieved, the expensive price and instability to failure have limited the practical application of this method [40,41]. Compared with a single growth factor, amniotic membranes are rich in collagen, cytokines, enzymes, and other active ingredients. In recent years, a new in-depth understanding of the biology of the amniotic membrane has emerged. Human amniotic tissue contains numerous growth factors, such as TGF-β1, bFGF, IGF-1, PDGF, and VEGF, which are vital regulators of tendon injury repair and adhesion formation [42–46]. Given its origin in human tissue, the composition and ratio of the promoter and inhibitor factors contained in the amniotic membrane are consistent with those of the human body. All these factors make amniotic membrane treatment of tendon injury always a hot research topic in recent years. Our results suggest that celecoxib reduces collagen synthesis, whereas amniotic membrane attenuates this tendency and improves the quality of tendon healing.

The PCL/AM-8% composite film has shown good results in preventing tendon adhesions, but some aspects of the study still need to be improved. Each of the abovementioned materials and celecoxib have its own advantages and disadvantages in application, and the precise use of two or more materials to build a tissue engineering scaffold that is conducive to tendon injury repair is still the focus of our next research. In addition, 3 weeks postoperatively is a critical period to achieve tendon healing and the beginning of clinical rehabilitation, which is also sufficient time to perform preliminary studies on this composite membrane. However, the effect of complete degradation of this membrane on long-term tendon healing and anti-adhesion has not been demonstrated. Therefore, this may be a direction for our future research.

5. Conclusions

Tendon adhesions are a natural part of the healing of tendon injuries, which seriously affect the functional recovery of patients. To date, the exact mechanism of adhesion has not been elucidated, and no effective treatment has been found. Drug-loaded absorbable polymeric membranes are considered to be effective and easy treatment strategies, but these methods do not create a suitable extracellular microenvironment for tendon repair and do not regulate the physiological processes of repair. The PCL/AM composite membrane loaded with celecoxib can continuously release celecoxib during the first 3 weeks of tendon repair to reduce the inflammatory response and deliver growth factors to the damaged area to build a suitable microenvironment for tendon repair, which provides a new direction to improve the repair efficiency of tendon tissue and avoid complications such as tendon adhesions.

Data availability statement

Datasets are either deposited in Figshare (https://doi.org/10.6084/m9.figshare.24581475) or presented in the main manuscript or supplementary files.

Ethical statement

All experiments were conducted in accordance with the institutional guidelines. The discarded placenta was the source of amniotic membranes, and informed consent was obtained from the pregnant woman (Ethics No. G2020-022-1). All animal procedures were approved by the Ethics Board of the Third Hospital of Hebei Medical University, with the approval number: Z2018-009-1.

CRediT authorship contribution statement

Chunjie Liu: Writing – original draft, Project administration, Investigation, Data curation, Conceptualization. **Xiaochong Zhang:** Methodology, Conceptualization. **Lili Zhao:** Validation, Software, Investigation. **Limin Hui:** Visualization, Validation, Software. **Dengxiang Liu:** Writing – review & editing, Project administration, Formal analysis, Conceptualization.

Declaration of competing interest

The authors declare that they have no known competing financial interests or personal relationships that could have appeared to influence the work reported in this paper.

Acknowledgements

This study was funded by the Natural Science Foundation of Hebei Province [NO. H2020105015]; Hebei Province Postdoctoral Science Foundation [NO. B2021003045]; and the Hebei Province Talent Project Funded Project [NO. A202101133].

Appendix A. Supplementary data

Supplementary data to this article can be found online at https://doi.org/10.1016/j.heliyon.2023.e23214.

References

[1] E. Vitale, C. Ledda, R. Adani, M. Lando, M. Bracci, E. Cannizzaro, L. Tarallo, V. Rapisarda, Management of high-pressure injection hand injuries: a multicentric, retrospective, observational study, J. Clin. Med. 8 (11) (2019), 2000.
[2] S. Polinder, G.I. Iordens, M.J. Panneman, D. Eygendaal, P. Patka, D. Den Hartog, E.M. Van Lieshout, Trends in incidence and costs of injuries to the shoulder, arm and wrist in The Netherlands between 1986 and 2008, BMC Publ. Health 13 (2013) 531.
[3] A.E. Loiselle, M. Kelly, W.C. Hammert, Biological augmentation of flexor tendon repair: a challenging cellular landscape, J Hand Surg Am 41 (1) (2016) 144–149.
[4] J.B. Tang, Clinical outcomes associated with flexor tendon repair, Hand Clin. 21 (2) (2005) 199–210.
[5] C.J. Dy, A. Hernandez-Soria, Y. Ma, T.R. Roberts, A. Daluiski, Complications after flexor tendon repair: a systematic review and meta-analysis, J Hand Surg Am 37 (3) (2012) 543–551.
[6] P. Amadio, K.N. An, A. Ejeskar, J.C. Guimberteau, S. Harris, R. Savage, K.S. Pettengill, J.B. Tang, IFSSH flexor tendon committee report, J. Hand Surg. 30 (1) (2005) 100–116.
[7] M. Tao, F. Liang, J. He, W. Ye, R. Javed, W. Wang, T. Yu, J. Fan, X. Tian, X. Wang, W. Hou, Q. Ao, Decellularized tendon matrix membranes prevent post-surgical tendon adhesion and promote functional repair, Acta Biomater. 134 (2021) 160–176.
[8] C.H. Chen, Y.H. Cheng, S.H. Chen, A.D. Chuang, J.P. Chen, Functional hyaluronic acid-polylactic acid/silver nanoparticles core-sheath nanofiber membranes for prevention of post-operative tendon adhesion, Int. J. Mol. Sci. 22 (2021) 8781.
[9] S. Liu, C. Hu, F. Li, X.J. Li, W. Cui, C. Fan, Prevention of peritendinous adhesions with electrospun ibuprofen-loaded poly(L-lactic acid)-polyethylene glycol fibrous membranes, Tissue Eng. 19 (2013) 529–537.
[10] L. Dong, L. Li, Y. Song, Y. Fang, J. Liu, P. Chen, S. Wang, C. Wang, T. Xia, W. Liu, L. Yang, MSC-derived immunomodulatory extracellular matrix functionalized electrospun fibers for mitigating foreign-body reaction and tendon adhesion, Acta Biomater. 133 (2021) 280–296.
[11] H. Maghsoudi, J. Hallajzadeh, M. Rezaeipour, Evaluation of the effect of polyphenol of escin compared with ibuprofen and dexamethasone in synoviocyte model for osteoarthritis: an in vitro study, Clin. Rheumatol. 37 (2018) 2471–2478.
[12] A.S. Hamy, S. Tury, X. Wang, J. Gao, J.Y. Pierga, S. Giacchetti, E. Brain, B. Pistilli, M. Marty, M. Espie, G. Benchimol, E. Laas, M. Lae, B. Asselain, B. Aouchiche, M. Edelman, F. Reyal, Celecoxib with neoadjuvant chemotherapy for breast cancer might worsen outcomes differentially by COX-2 expression and ER status: exploratory analysis of the REMAGUS02 trial, J. Clin. Oncol. 37 (2019) 624–635.
[13] S. Jiang, X. Zhao, S. Chen, G. Pan, J. Song, N. He, F. Li, W. Cui, C. Fan, Down-regulating ERK1/2 and SMAD2/3 phosphorylation by physical barrier of celecoxib-loaded electrospun fibrous membranes prevents tendon adhesions, Biomaterials 35 (2014) 9920–9929.
[14] O. Dolkart, T. Liron, O. Chechik, D. Somjen, T. Brosh, E. Maman, Y. Gabet, Statins enhance rotator cuff healing by stimulating the COX2/PGE2/EP4 pathway: an in vivo and in vitro study, Am. J. Sports Med. 42 (2014) 2869–2876.
[15] V.R. Patel, S. Samavedi, A.S. Bates, A. Kumar, R. Coelho, B. Rocco, K. Palmer, Dehydrated human amnion/chorion membrane allograft nerve wrap around the prostatic neurovascular bundle accelerates early return to continence and potency following robot-assisted radical prostatectomy: propensity score-matched analysis, Eur. Urol. 67 (2015) 977–980.
[16] J. Delaey, L. De Vos, C. Koppen, P. Dubruel, S. Van Vlierberghe, B. Van den Bogerd, Tissue engineered scaffolds for corneal endothelial regeneration: a material's perspective, Biomater. Sci. 10 (2022) 2440–2461.
[17] H. Elkhenany, A. El-Derby, M. Abd Elkodous, R.A. Salah, A. Lotfy, N. El-Badri, Applications of the amniotic membrane in tissue engineering and regeneration: the hundred-year challenge, Stem Cell Res. Ther. 13 (2022) 8.
[18] T.J. Koob, R. Rennert, N. Zabek, M. Massee, J.J. Lim, J.S. Temenoff, W.W. Li, G. Gurtner, Biological properties of dehydrated human amnion/chorion composite graft: implications for chronic wound healing, Int. Wound J. 10 (2013) 493–500.
[19] D.J. Yang, F. Chen, Z.C. Xiong, C.D. Xiong, Y.Z. Wang, Tissue anti-adhesion potential of biodegradable PELA electrospun membranes, Acta Biomater. 5 (7) (2009) 2467–2474.
[20] J.A. Blin, R.M. Ali, A. Nurdin, R.A. Hamid, Quinone-rich fraction of Ardisia crispa (Thunb.) A. DC roots alters angiogenic cascade in collagen-induced arthritis, Inflammopharmacology 29 (2021) 771–788.
[21] H. Chen, Z. Qian, S. Zhang, J. Tang, L. Fang, F. Jiang, D. Ge, J. Chang, J. Cao, L. Yang, X. Cao, Silencing COX-2 blocks PDK1/TRAF4-induced AKT activation to inhibit fibrogenesis during skeletal muscle atrophy, Redox Biol. 38 (2021), 101774.
[22] M.G. Grewal, C.B. Highley, Electrospun hydrogels for dynamic culture systems: advantages, progress, and opportunities, Biomater. Sci. 9 (2021) 4228–4245.
[23] L. Dejob, B. Toury, S. Tadier, L. Gremillard, C. Gaillard, V. Salles, Electrospinning of in situ synthesized silica-based and calcium phosphate bioceramics for applications in bone tissue engineering: a review, Acta Biomater. 123 (2021) 123–153.
[24] E. Garcia-Melchor, G. Cafaro, L. MacDonald, L.A.N. Crowe, S. Sood, M. McLean, U.G. Fazzi, I.B. McInnes, M. Akbar, N.L. Millar, Novel self-amplificatory loop between T cells and tenocytes as a driver of chronicity in tendon disease, Ann. Rheum. Dis. 80 (2021) 1075–1085.
[25] A. Liu, Q. Wang, Z. Zhao, R. Wu, M. Wang, J. Li, K. Sun, Z. Sun, Z. Lv, J. Xu, H. Jiang, M. Wan, D. Shi, C. Mao, Nitric oxide nanomotor driving exosomes-loaded microneedles for achilles tendinopathy healing, ACS Nano 15 (2021) 13339–13350.
[26] C. Cai, X. Zhang, Y. Li, X. Liu, S. Wang, M. Lu, X. Yan, L. Deng, S. Liu, F. Wang, C. Fan, Self-healing hydrogel embodied with macrophage-regulation and responsive-gene-silencing properties for synergistic prevention of peritendinous adhesion, Adv. Mater. 34 (2022), e2106564.
[27] J.Y. Sunwoo, C.D. Eliasberg, C.B. Carballo, S.A. Rodeo, The role of the macrophage in tendinopathy and tendon healing, J. Orthop. Res. 38 (2020) 1666–1675.
[28] Q.Q. Yang, L. Zhang, Y.L. Zhou, J.B. Tang, Morphological changes of macrophages and their potential contribution to tendon healing, Colloids Surf. B Biointerfaces 209 (2022), 112145.
[29] A.K. Greene, I.P. Alwayn, V. Nose, E. Flynn, D. Sampson, D. Zurakowski, J. Folkman, M. Puder, Prevention of intra-abdominal adhesions using the antiangiogenic COX-2 inhibitor celecoxib, Ann. Surg. 242 (2005) 140–146.
[30] F. Li, B. He, S. Liu, C. Fan, Celecoxib effectively inhibits the formation of joint adhesions, Exp. Ther. Med. 6 (2013) 1507–1511.
[31] K. Kawasaki, K. Kurahara, S. Yanai, S. Kochi, T. Fuchigami, T. Matsumoto, Low-dose aspirin and non-steroidal anti-inflammatory drugs increase the risk of bleeding in patients with gastroduodenal ulcer, Dig. Dis. Sci. 60 (2015) 1010–1015.
[32] F.A. Sass, M. Fuchs, M. Pumberger, S. Geissler, G.N. Duda, C. Perka, K. Schmidt-Bleek, Immunology guides skeletal muscle regeneration, Int. J. Mol. Sci. 19 (2018) 835.
[33] T. Stauber, M. Wolleb, A. Duss, P.K. Jaeger, I. Heggli, A.A. Hussien, U. Blache, J.G. Snedeker, Extrinsic macrophages protect while tendon progenitors degrade: insights from a tissue engineered model of tendon compartmental crosstalk, Adv. Healthcare Mater. 10 (2021), e2100741.
[34] K.L. Howell, D.A. Kaji, T.M. Li, A. Montero, K. Yeoh, P. Nasser, A.H. Huang, Macrophage depletion impairs neonatal tendon regeneration, Faseb. J. 35 (2021), e21618.
[35] R. Ramakrishnan, H.V. Sreelatha, A. Anil, S. Arumugham, P. Varkey, M. Senan, L.K. Krishnan, Human-derived scaffold components and stem cells creating immunocompatible dermal tissue ensuing regulated nonfibrotic cellular phenotypes, ACS Biomater. Sci. Eng. 6 (2020) 2740–2756.
[36] I.A. Deus, J.F. Mano, C.A. Custodio, Perinatal tissues and cells in tissue engineering and regenerative medicine, Acta Biomater. 110 (2020) 1–14.
[37] C.H. Lee, F.Y. Lee, S. Tarafder, K. Kao, Y. Jun, G. Yang, J.J. Mao, Harnessing endogenous stem/progenitor cells for tendon regeneration, J. Clin. Invest. 125 (2015) 2690–2701.
[38] B. Han, I.A. Jones, Z. Yang, W. Fang, C.T. Vangsness Jr., Repair of rotator cuff tendon defects in aged rats using a growth factor injectable gel scaffold, Arthroscopy 36 (2020) 629–637.
[39] M. Aynardi, T. Zahoor, R. Mitchell, J. Loube, T. Feltham, L. Manandhar, S. Paudel, L. Schon, Z. Zhang, Orthotopic transplantation of achilles tendon allograft in rats: with or without incorporation of autologous mesenchymal stem cells, Cell Transplant. 27 (2018) 245–255.
[40] S. Vermeulen, Z. Tahmasebi Birgani, P. Habibovic, Biomaterial-induced pathway modulation for bone regeneration, Biomaterials 283 (2022), 121431.

[41] S. Ruiz-Alonso, M. Lafuente-Merchan, J. Ciriza, L. Saenz-Del-Burgo, J.L. Pedraz, Tendon tissue engineering: cells, growth factors, scaffolds and production techniques, J. Contr. Release 333 (2021) 448–486.
[42] R. Sarvari, P. Keyhanvar, S. Agbolaghi, L. Roshangar, E. Bahremani, N. Keyhanvar, M. Haghdoost, S.H. Keshel, A. Taghikhani, N. Firouzi, A. Valizadeh, E. Hamedi, M. Nouri, A comprehensive review on methods for promotion of mechanical features and biodegradation rate in amniotic membrane scaffolds, J. Mater. Sci. Mater. Med. 33 (2022) 32.
[43] N.L. Millar, K.G. Silbernagel, K. Thorborg, P.D. Kirwan, L.M. Galatz, G.D. Abrams, G.A.C. Murrell, I.B. McInnes, S.A. Rodeo, Tendinopathy. Nature reviews. Disease primers 7 (2021) 1.
[44] A. Prabhath, V.N. Vernekar, C.J. Esdaille, E. Eisenberg, A. Lebaschi, M. Badon, A. Seyedsalehi, G. Dzidotor, X. Tang, N. Dyment, S. Thomopoulos, S.G. Kumbar, A. Deymier, E. Weber, C.T. Laurencin, Pegylated insulin-like growth factor-1 biotherapeutic delivery promotes rotator cuff regeneration in a rat model, J. Biomed. Mater. Res. 110 (2022) 1356–1371.
[45] H. Tempfer, G. Spitzer, C. Lehner, A. Wagner, R. Gehwolf, J. Fierlbeck, N. Weissenbacher, M. Jessen, L.M. Heindl, A. Traweger, VEGF-D-mediated signaling in tendon cells is involved in degenerative processes, Faseb. J. 36 (2022), e22126.
[46] O. Evrova, G.M. Burgisser, C. Ebnother, A. Adathala, M. Calcagni, E. Bachmann, J.G. Snedeker, C. Scalera, P. Giovanoli, V. Vogel, J. Buschmann, Elastic and surgeon friendly electrospun tubes delivering PDGF-BB positively impact tendon rupture healing in a rabbit Achilles tendon model, Biomaterials 232 (2020), 119722.